Ion beam sputtered nanostructured semiconductor surfaces as templates for nanomagnet arrays



2009 J. Phys.: Condens. Matter 21 224025

(http://iopscience.iop.org/0953-8984/21/22/224025)

J. Phys.: Condens. Matter **21** (2009) 224025 (9pp) doi:10.1088/0953-8984/21/22/224025

# Ion beam sputtered nanostructured semiconductor surfaces as templates for nanomagnet arrays

**C Teichert[1,5], J J de Miguel[2,3] and T Bobek[4,6]**

[1] Institute of Physics, University of Leoben, 8700 Leoben, Austria
[2] Department of Condensed Matter Physics, Universidad Autónoma de Madrid, Cantoblanco, 28049 Madrid, Spain
[3] Institute of Materials Science 'Nicolás Cabrera', Cantoblanco, 28049 Madrid, Spain
[4] Institute of Semiconductor Technology, University of Aachen, 52074 Aachen, Germany

E-mail: teichert@unileoben.ac.at

Received 8 January 2009
Published 12 May 2009
Online at stacks.iop.org/JPhysCM/21/224025

**Abstract**

The ongoing tendency for increasing the storage densities in magnetic recording techniques requires a search for efficient routes to fabricate and characterize nanomagnet arrays on solid supports. Spontaneous pattern formation in semiconductor heteroepitaxy or under ion erosion of semiconductor surfaces yields nanostructured substrates that can serve as templates for subsequent deposition of magnetic material. The nanostructured morphology of the template can easily be replicated into the magnetic coating by means of the shadow deposition technique which allows one to selectively cover specific areas of the template with magnetic material. Here, we demonstrate that ion bombardment induced hexagonally arranged GaSb dots are suitable templates for fabricating by shadow deposition close-packed nanomagnets with a lateral extension of $\leqslant$50 nm, i.e. with a resulting storage density of up to 0.2 Tbit in$^{-2}$. Magnetic-force microscopy (MFM) measurements revealed that the individual nanomagnets—which are located on the tops of the semiconductor hillocks—are single domain and show mainly independent magnetization. The coupling behaviour was estimated from correlation function analysis of the MFM data. In addition, magneto-optical Kerr effect measurements demonstrate that the nanomagnets can be magnetized either out-of-plane or in-plane and show remanence at room temperature, with a coercive field of 120 mT.

(Some figures in this article are in colour only in the electronic version)

## 1. Introduction

The rapidly increasing demand for ever smaller structures in information technologies requires effective techniques for generating regular arrangements of nano-objects. Besides quantum dots for optoelectronic applications, magnetic nanoparticles for data storage applications are of particular importance [1]. As an alternative to costly lithographical methods or to slow serial processing, as in electron beam lithography or focused ion beam machining, spontaneous pattern formation in semiconductor heteroepitaxy [2] or during noble gas ion sputtering [3] yields quasi periodic nanostructured surfaces that may serve as large area templates, e.g. for subsequent deposition of magnetic material [4]. In fact a decade ago it was demonstrated for self-organized {105} facetted SiGe/Si(001) films (for a recent review see [5]) that shadow deposition of magnetic material on self-organized semiconductor templates is quite a smart way to generate arrays of chemically isolated nanomagnets with lateral dimensions of a few tens of nanometres [6]. The results obtained by depositing pure Co onto one of the three occurring nanofacet orientations are demonstrated in figure 1. Magneto-optical Kerr effect (MOKE) investigations proved that the parallelogram-shaped 25 nm × 35 nm × 2 nm Co nanomagnets are single domain with the easy

[5] Author to whom any correspondence should be addressed.
[6] Present address: VDI Technologiezentrum GmbH, 40468 Düsseldorf, Germany.

 

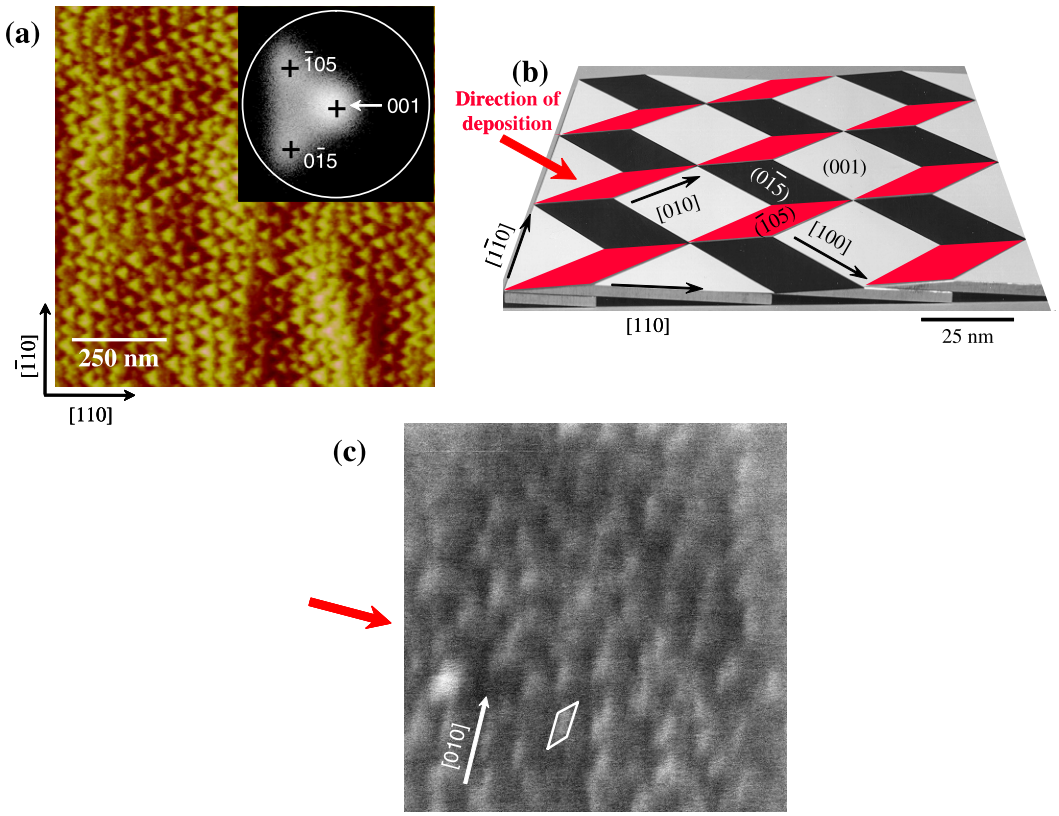


**Figure 1.** (Colour online) (a) 1 $\mu$m × 1 $\mu$m AFM image of a 2.5 nm $Si_{0.55}Ge_{0.45}$ film grown on a vicinal Si(001) substrate with a 4° polar miscut along [ $\bar{1}\bar{1}$0] ($z$-scale: 5 nm). The inset shows a 15° polar plot presentation of the histogram of orientation of surface normals indicating the presence of two orientations of {105} facets as well as (001) terraces. (b) Scheme of shadow deposition. For glancing incidence deposition along the indicated direction (thick arrow) only the 35 nm × 25 nm large parallelogram-shaped ($\bar{1}$05) facets will be covered with magnetic material. (c) 360 nm × 360 nm scanning electron micrograph of the template shown in (a) after shadow deposition with a 2 nm Co/2 nm Cu bilayer. The thick arrow denotes the (projected) orientation of the evaporation and the white parallelogram denotes size and orientation of the Co covered ($\bar{1}$05) facets which appear bright due to the higher secondary electron yield of Co compared to that of the uncoated SiGe film. (After [4].)

axis of magnetization along their long axis [6]. In the meantime, similar nanofacetted heteroepitaxial SiGe templates allow one to image the magnetization and to study the interparticle coupling of the shadow deposited nanomagnet arrays by photoemission electron microscopy with x-ray magnetic circular dichroism contrast [7, 8].

Ion beam sputtering, too, has the potential to fabricate nanomagnet arrays, because this massive-parallel fabrication method is a promising alternative to existing nanostructuring techniques. Recently, ion beam erosion was successfully used to nanostructure magnetic coatings on both metal and semiconductor supports [9, 10]. In analogy to the heteroepitaxial semiconductor nanostructures, ion bombardment induced surface patterns may also serve as templates for nanomagnet arrays. In particular, hexagonally arranged dot patterns on III–V semiconductors [3]—which originate from an interplay of sputtering processes and surface diffusion (see [11–14] and articles in this special volume)—may be used as templates for shadow deposition as proposed recently [4].

The situation for shadow deposition of magnetic material onto an ion bombardment induced self-organized array of semiconductor nanostructures is sketched in figure 2. Figure 2(a) shows an atomic-force microscopy (AFM) image of an originally smooth GaSb(001) wafer which was irradiated at temperatures below 100 °C with $Ar^+$ ions of 500 eV kinetic energy under a perpendicular angle of incidence until saturation in surface roughness was reached [13]. The surface morphology displays domains of hexagonally close-packed dots. From the two-dimensional (2D) power spectral density (PSD) analysis (inset of figure 2(a)) it can be deduced that these domains are isotropically arranged with respect to each other resulting in rings in the 2D PSD rather than a hexagonal pattern. The number of higher order rings is a measure of the domain size. The mean lateral dot distance and its uniformity can be determined from the radius and width of the first ring. Because of the isotropy of the domain orientation here the radial power spectral density can also be analysed [13], yielding a mean inter-dot distance of 50 nm ± 5 nm. Figure 2(b) presents a high-resolution AFM image recorded with a carbon nanotube tip, revealing uniformly shaped dots with heights up to 25 nm [15]. The image also demonstrates that the dots touch each other, i.e. we have domains of close-packed 50 nm diameter dots. The existence of gradually changing side slopes of the dots in contrast to a nanofacetted surface morphology is supported by the observation of a 2 nm thick amorphous layer after ion irradiation [16].

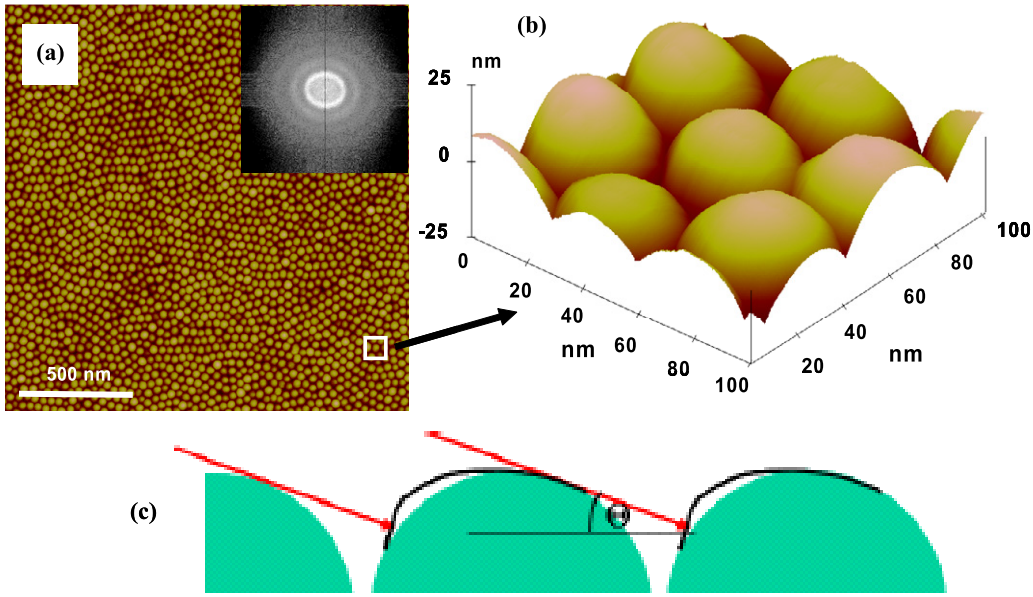


**Figure 2.** (Colour online) (a) 2 $\mu$m × 2 $\mu$m AFM image of a 500 eV $Ar^+$ bombarded GaSb(111) surface ($z$-scale: 50 nm). The inset represents the corresponding 2D power spectral density. (After [13].) (b) High-resolution AFM image of the marked area in (a) recorded with a carbon nanotube tip (from [4]). (c) Scheme of the resulting Co coverage (black curves) after shadow deposition under $\theta = 20°$ from the left.

Using the shadow deposition technique, nanomagnet arrays have been fabricated that closely replicate the template dot pattern. When the magnetic material is deposited under an oblique angle (in our case cobalt under 20°) onto such dot arrays only a calotte like area on the tops of the dots will be exposed to the incident beam due to the partial shadowing caused by the surface topography. Figure 2(c) illustrates schematically the expected cross section of the magnetic cap as it results from the varying angle of incidence. By comparing figures 2(a)–(c) one can assume that shadow deposition will result in a close-packed array of chemically isolated magnetic nanostructures. Their shape is similar to a curved circular disc with calotte like surfaces with a diameter of about 30 nm. As we shall see, the curved shape of the nanomagnets produced in these experiments will result in a specific magnetic behaviour and establish a clear difference with respect to the planar ones previously fabricated by shadow deposition on nanofacetted heteroepitaxial semiconductor films. The particular size and shape of the individual nanomagnets will of course depend on the distinct arrangement of adjacent dots with deposition direction.

The magnetic material chosen was a Pt/Co/Pt trilayer, because of its magnetic hardness, as explained in more detail below. Magnetic-force microscopy (MFM) measurements revealed that the nanomagnets are single domain with magnetization uncorrelated with those of their neighbours, as could be determined by correlation function analysis of the MFM data. MOKE investigations in longitudinal and polar geometry (with respect to the overall template surface) revealed that the easy axis of magnetization lies nearly out-of-plane. The results of the magnetic characterization clearly demonstrate the potential of self-organized ion beam sputtered semiconductor surfaces as templates to fabricate high-density magnetic storage devices.

## 2. Experimental details

The self-organized semiconductor template was fabricated by bombarding commercially available GaSb(100) wafers under normal incidence with 500 eV $Ar^+$-ions (ion current density of about $10^{15}$ $cm^{-2}$ $s^{-1}$) using a Leybold INA3 sputtered neutral mass spectrometer (SNMS) until a stationary pattern was obtained. The experimental details are described elsewhere [13]. The morphology of the GaSb dot pattern was measured *ex situ* by atomic-force microscopy (AFM) in tapping mode using plasma-shaped high-density carbon (HDC) tips and carbon nanotube (CNT) tips as probes. After transferring the template to a molecular beam epitaxy (MBE) system operating in ultra-high vacuum, the Pt/Co/Pt trilayers were deposited at room temperature employing electron bombardment evaporators; the pressure during deposition was held below $1 \times 10^{-9}$ mbar. The substrate was degreased by rinsing with ethanol prior to inserting into a vacuum; no further treatment was applied to the surface template prior to deposition, i.e. the native oxide on the surface was not removed. The deposition rates were calibrated by monitoring the specularly reflected intensity of a neutral He beam on a Cu(100) substrate [17]. The Co thickness (18 ML) was chosen in order to have a strong out-of-plane magnetization, as monitored during growth by *in situ* MOKE measurements. Co was deposited under a polar angle of incidence of 20° to achieve a proper shadow effect. The embedding Pt layers were grown at a higher incidence of 45° to ensure a rather homogeneous coverage on the GaSb dots and of the Co

deposits. The Pt layer was rather thick (15 ML) to avoid oxidation of the Co film.

The AFM/MFM measurements after MBE deposition were performed under ambient conditions using an MFP-3D AFM with a closed loop scanner from Asylum Research. Nanosensors PPP-LM-MFMR tips were used as magnetic probes. They are coated with a low moment, hard magnetic CoCr film which is out-of-plane magnetized, i.e. the setup is mainly sensitive to out-of-plane magnetization with respect to the template's average surface. Due to the magnetic coating the tip radius is about 30 nm. In MFM mode for each scan the topography is first recorded; subsequently for an increased tip–sample distance the phase shift between cantilever oscillation and cantilever excitation due to the magnetic stray field from the sample is recorded. This phase shift in degrees is presented in the MFM images [18]. Magnetic-force microscopy measurements on such rough samples, as in our case, are difficult to perform because of topographical artefacts. Therefore, the probe was retracted in MFM mode for the maximum distance from the actual surface—still allowing feedback—to record magnetic interaction between sample and probe while minimizing the influence of the surface topography.

The magnetic characterization of the samples was carried out by means of MOKE measurements. Two different setups were used: one operating *in situ* at the growth chamber and under UHV conditions, with a maximum applicable field of 60 mT, and another one *ex situ*, allowing for sample polar and azimuthal rotation to fully determine the magnetic anisotropy [10]. The highest magnetic field available in the latter experimental system is 0.35 T, and the probe laser beam can be focused down to a diameter of 100 $\mu$m.

## 3. Results and discussion

### *3.1. Some general considerations about nanomagnetism*

When dealing with magnetic objects of nanometre dimensions, several issues must be kept in mind:

(i) *Superparamagnetism*. As the dimensions of the object become progressively smaller a fundamental limitation arises, since thermal fluctuations can overcome the ordering effect of exchange coupling and the magnetic moments tend to disorder spontaneously. This state is called superparamagnetism, and it severely limits the possible applications and the useful temperature ranges of these materials.

(ii) *Magnetic anisotropy*. The existence of energetically preferred directions for the alignment of the magnetic moments is intimately linked to the spatial arrangement of the interacting atoms within the material's crystalline structure; this is therefore a typical example of a property that must be expected to change substantially as the material's dimensions are reduced from bulk to nanometre scale, and the environment of the magnetic atoms is altered. In general, the reduced dimensions and symmetries in these nanometre objects will also result in a reduction of the anisotropy energy [8], thus favouring the onset of superparamagnetism since the barrier that the magnetization must overcome to flip direction becomes smaller.

(iii) *Interparticle coupling*. The magnetostatic interactions between adjacent particles in an array can in general be neglected for separations larger than ∼100 nm; nevertheless, they can become dominant on the 10 nm scale and under these conditions, with a reduced anisotropy and an increasingly unstable magnetization of each individual nanomagnet [19], thus determining the ground state of the system [20].

The nanodot templates produced by ion bombardment are particularly attractive for applications in nanomagnetism because the characteristic dot sizes attainable naturally fall in the range for which single domain behaviour is expected. On the other hand, these dimensions are also rather close to the superparamagnetic limit for many materials, and the short separations between the nanomagnets are likely to result in strong interparticle dipolar coupling. Indeed, previous experiments in which Co dots were produced by shadow deposition onto self-organized SiGe substrates revealed that the magnetizations of the Co nanoislands were not independently oriented, but rather grouped in micrometre-sized domains [7]. This phenomenon is obviously undesirable for possible applications such as high-density magnetic recording media or sensors. One possible strategy for achieving individually magnetized dots is to substitute the Co for other magnetic materials, or combinations of them, presenting a higher magnetic anisotropy and a stronger coercivity, in such a way that the magnetic status of one nanomagnet cannot be reversed by the interaction with its neighbours. In particular, the Co/Pt multilayer system, with its high magnetic hardness and strong perpendicular anisotropy [21, 22], is a promising candidate for the production of magnetic nanodots in the range of sizes and separations characteristic of dot templates created by ion erosion.

### *3.2. AFM/MFM analysis of the sample topography and magnetic structure*

Figure 3 presents the topography of the template after shadow deposition with a Pt/Co/Pt trilayer and the MFM signal taken on the same part of the surface. From the 2D PSD of a larger topography measurement (see inset in figure 3(a)) one can derive the average distance of the coated dots to be 50 nm as for the bar template. The decrease in the measured height of the dots is attributed to the rather large MFM tip radius which does not allow penetration between the dots as was possible for the CNT tip used to record figure 2(b). The MFM image shown in figure 3(b) reveals circular dark and bright areas representing the individual nanomagnets which correspond to the GaSb dot locations. Within most of the areas the contrast is changing only slightly, hinting at out-of-plane anisotropy of the magnetization of these nanomagnets. It should be noted that only in one case out of dozens of MFM images was an abrupt change in phase contrast on top of a larger dot—indicating a nanomagnet with two domains—observed. Thus the AFM data strongly support the assumption

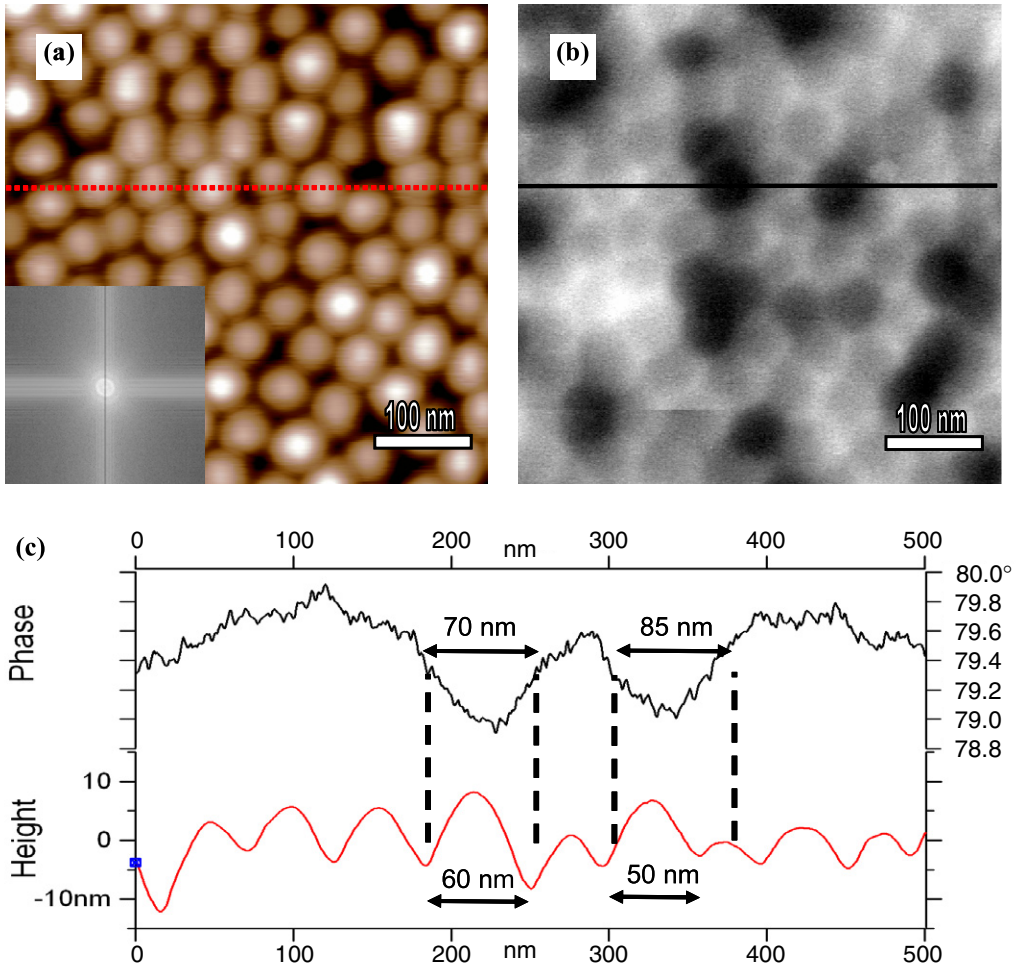


**Figure 3.** (Colour online) (a) 500 nm × 500 nm AFM image of the template shown in figure 2 after coverage with a 18 ML Pt/15 ML Co/18 ML Pt trilayer ($z$-scale: 20 nm). The inset corresponds to the 2D PSD calculated from a 1 $\mu$m × 1 $\mu$m image to improve the statistics. (b) Corresponding MFM image (phase scale: 1°). (c) Line sections through the lines marked in (a) and (b). Lower line, topography; upper line, corresponding MFM contrast.

that the fabricated nanomagnets are almost exclusively single domain particles, as was to be expected for these dot sizes and given the high magnetic anisotropy of the Pt/Co/Pt trilayers. The comparison of the corresponding line scans (figure 3(c)) clearly demonstrates the magnetic origin of the dominating phase contrast, i.e. there are adjacent topographic protrusions which result in opposite magnetic contrast. The fact that the lateral size of the detected phase information is on average 20–30 nm larger than the dot diameter is attributed to the interaction of the rather dull MFM tip used with the stray fields emanating from the surface. Some of the light grey areas which are presumably not out-of-plane magnetized (see below) are surrounded by bright rings. The origin of these rings is attributed to the influence of the topography on the phase shift, when the tip is measuring the deep depression between the dots.

Figure 3(b) shows several neighbouring dots with the same MFM signal, i.e. there are areas with a lateral extension of up to 250 nm within which the nanomagnets exhibit the same magnetization. To quantify this magnetic coupling of the dots, two different types of analysis were carried out.

First, the number of dot pairs within a distance of 75 nm from the centre of each dot was manually counted, using a 1 $\mu$m × 1 $\mu$m MFM image. The fraction of dot pairs showing opposite contrast in the MFM image is 53%. This value reflects the tendency of independent magnetization of adjacent nanomagnets and low coupling.

Also correlation function analysis of topographic and magnetic images allows us to quantify the effect of magnetic coupling between the nanomagnets. Analysis of the height–height correlation function $C$ and of the height-difference function $H$ is usually applied for comprehensive roughness characterization of random rough surfaces [23]. This includes the root-mean-square roughness $\sigma$ as a measure of the vertical roughness fluctuations, the lateral correlation length $\xi$, and the roughness exponent $\alpha$. The correlation length $\xi$ indicates the distance within which the heights of two surface points are correlated. It yields information on the lateral roughness fluctuations and is a measure for the minimum lateral feature

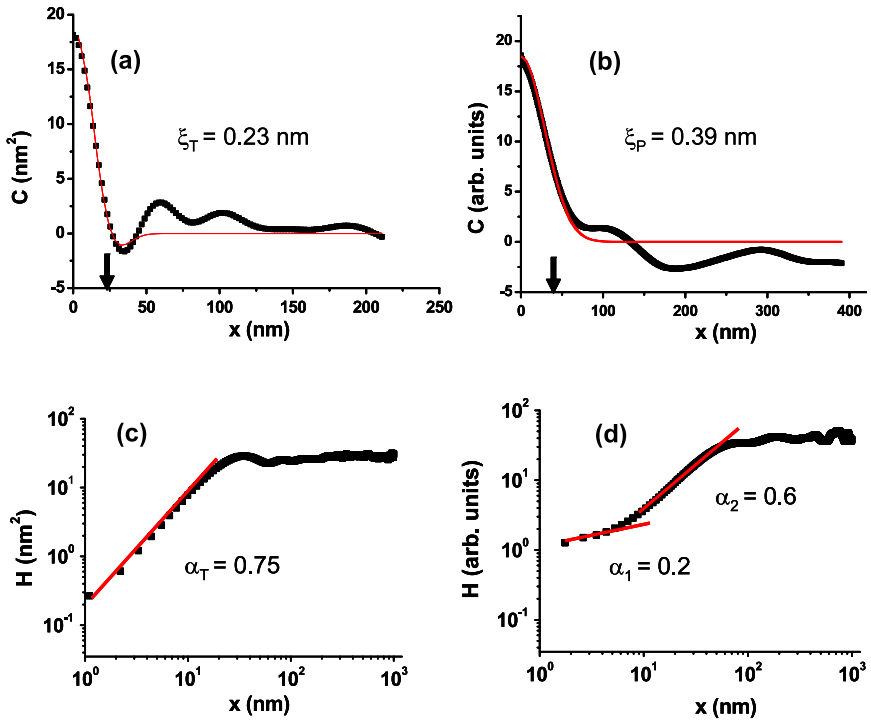


**Figure 4.** (Colour online) The height–height-correlation function $C(x)$ calculated from (a) a 1 $\mu$m × 1 $\mu$m AFM image and (b) the corresponding MFM signal which were measured at the same position as shown in figure 3. The thin lines are the corresponding fits to equations (4) and (3), respectively. The arrows indicate $\xi_T$ and $\xi_P$, respectively. Note the different scales. (c), (d) Height-difference function $H(x)$ calculated from the AFM image and from the MFM image, respectively. The red lines mark the initial slope for $x \ll \xi$, which is used to calculate the Hurst parameter $\alpha$.

size. The roughness exponent $\alpha$, also called the Hurst parameter, is related to the local fractal dimension. Its value usually ranges from 1 to 0.5, the latter describing a more jagged surface. For an isotropic surface without a directional dependence of the roughness, the one-dimensional height–height-correlation function $C(x)$ can be easily calculated from the AFM data

$$C(x) = \langle [z(x_0 + x) - \langle z \rangle][z(x_0) - \langle z \rangle] \rangle \tag{1}$$

where $\langle\,\rangle$ denotes the average value and $z(x_0)$ is the height at a surface point $x_0$.

In analogy the 1D height-difference function $H(x)$ is calculated as

$$H(x) = \langle [z(x_0 + x) - z(x_0)]^2 \rangle. \tag{2}$$

For a self-affine fractal surface, $C(x)$ can be written as

$$C(x) = \sigma^2 \exp[-(|x|/\xi)^{2\alpha}] \tag{3}$$

allowing easy determination of $\xi$ [23]; $H(x)$ shows an exponential behaviour $H(x) \sim x^{2\alpha}$ in the limit $x \ll \xi$, which allows us to determine $\alpha$ as the initial slope of the curve from a log–log plot of $H(x)$ [23]. For a mounded surface topography, as in our case, a more appropriate fit for $C(x)$ is

$$C(x) = \sigma^2 \exp[-(|x|/\xi)^{2\alpha}] \cos(2\pi x/\lambda) \tag{4}$$

where $\lambda$ corresponds to the average mound separation [23].

In figure 4 we demonstrate that correlation function analysis applied to both the height signal in topographic images and to the phase signal in the MFM image allows us to quantify the influence of the magnetic coupling between the nanomagnets on the relative alignment of their magnetizations. In figures 4(a), (b) the height–height-correlation functions are presented. For the topography the lateral correlation length $\xi_T = 23$ nm was determined using equation (4), whereas for the MFM image the best fit was obtained for equation (3) resulting in a correlation length $\xi_P = 39$ nm. This larger value can again be put down to the interaction of the rather dull MFM tip used with the stray fields emanating from the surface. From the ratio of $\xi$ for both images ($\xi_P/\xi_T = 1.7$), the apparent size of the single domain nanomagnets can be calculated. Using the lateral size of the dots—which is about 50 nm—the average diameter of the individual objects in the MFM image is calculated to be 85 nm, in agreement with line scan analysis presented in figure 3. The Hurst parameter $\alpha$, determined from the height-difference functions of both the topographic and the MFM image, is used to describe the transition between independently magnetized areas. From the topography image we found $\alpha_T = 0.75$ (figure 4(c)). However, for the MFM image two different initial slopes in the log–log presentation of the height-difference function are observed (figure 4(d)): a very shallow increase below 10 nm lateral distance and a range with a steeper slope between 10 and 100 nm. We have to recall that low values of $\alpha$ correspond to a more jagged surface or more sudden changes in the measured properties. Thus, a value of $\alpha_1 = 0.2$ for lateral distances below 10 nm is the result of

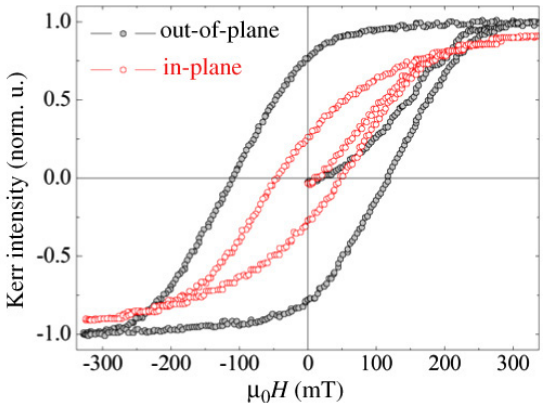


**Figure 5.** MOKE hysteresis loops measured *ex situ* on the same sample presented in figure 3 in polar configuration (black) and longitudinal configuration (red).

sudden changes in the magnetic signal between neighbouring dots. This again indicates the occurrence of a high percentage of adjacent nanomagnets with opposite magnetization, which is a signal of non-correlation (50% would be expected for a purely random distribution). The second value of $\alpha_2 = 0.6$ corresponds to the gradual change in magnetic contrast within a single domain magnet which is the result of the thickness fluctuations that are unavoidable given the deposition method and the morphology of the templates used (as schematically depicted in figure 2(c)).

The magnetic anisotropy of the fabricated nanomagnet array is revealed by the hysteresis loops measured *ex situ* and at room temperature by MOKE. Measurements have been performed in polar and longitudinal configuration to probe both the out-of-plane and in-plane component of the magnetization. As seen in figure 5, the sample could be saturated in both cases but the out-of-plane axis seems to be easier, since the loop shape is squarer and the remanence higher ($M_r/M_s = 0.77$) than when the magnetization lies in the surface plane ($M_r/M_s = 0.28$). The fact that the dots can be magnetized along both directions is to be assigned to the curved shape and the non-uniform thicknesses of the Pt/Co/Pt trilayer provoked by the deposition procedure, which must result in a distribution of interfaces with different orientations and magnetic anisotropies. This observation is in agreement with previous observations on nanomagnets obtained by oblique incidence deposition of Co/Pd multilayers on polystyrene spheres [24]. Recently, it has further been shown that, in nanometre-sized magnetic entities, structural relaxations can affect the magnetic anisotropy substantially [8].

Figure 6 displays a 3D presentation of an MFM measurement, where the phase shift was overlaid in false colour coding on the topography signal. The presentation reveals that besides single domain nanomagnets with clear magnetization (blue or red) some dots without detectable magnetization also appear. Dots which depict a phase shift below 0.33° and above 0.66° are supposed to be magnetized nearly out-of-plane. The percentage of these dots is about 60%. We suggest that the dots which appear green in figure 6 may have different Co thicknesses than the rest; if the amount of Co is smaller, their Curie temperature could be close to or below room temperature, and the dots would behave paramagnetically. Otherwise, if the Co thickness exceeds a certain limit a spin reorientation phase transition takes place that drives the system's magnetization into the surface plane [25]. In either case, these dots would yield a much weaker magnetic contrast in the MFM setup used. Although special care has been taken to calibrate and maintain constant fluxes of Co and Pt during deposition, the imperfect periodicity of the dot arrangement and the fluctuations in dot heights may explain why the shadow deposition onto this type of self-organized surface template leads to differences in the amount

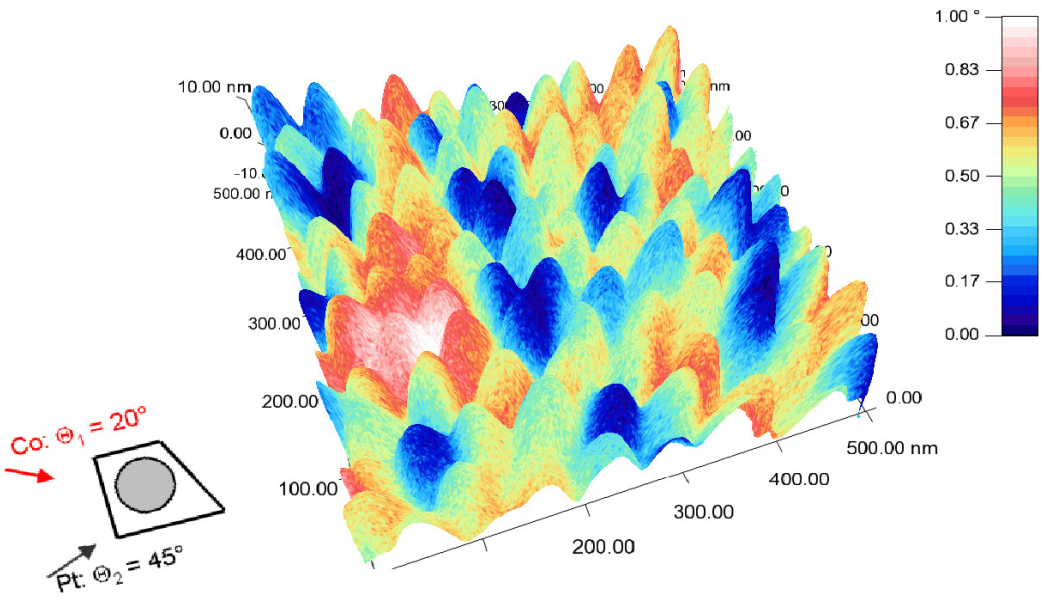


**Figure 6.** 3D presentation of the AFM/MFM measurement shown in figure 3. The phase shift of the MFM measurement is used as a colour code in a false colour presentation employing the ARGyle Software from Asylum Research. In the lower left, the projected angles of incidence of the Co and Pt deposition are indicated.

of material on different dots. It should be noted here that even for normal incidence of Co/Pd films on GaSb dots [26] the thickness fluctuations result in a reduced effective magnetic anisotropy. The advantage of the shadow deposition technique clearly lies in the possibility of creating chemically isolated magnetic 'caps' on the dots, thus allowing for a massively parallel fabrication of magnetically independent dots.

## 4. Conclusion and outlook

The shadow deposition technique applied on an ion bombardment induced, self-organized pattern of 50 nm diameter GaSb dots has been demonstrated to be an efficient way to fabricate a close-packed nanomagnet array. MFM and MOKE characterization reveal that the nanomagnets are single domain and preferentially out-of-plane magnetized. Correlation function analysis of the MFM data revealed little interparticle magnetic coupling. Thus, the proposed application of ion beam sputtered nanostructured semiconductor surfaces bears the potential to fabricate magnetic storage media with a storage density of at least 0.2 Tbit in$^{-2}$. The necessary periodicity of the template (and therefore in the nanomagnet array) might be achieved by a prestructuring on the $\mu$m-scale [27, 28]. The storage density can be further increased by reducing the dot size of the ion bombarded template beyond the 50 nm occurring in our model template. As the lateral dot size can be tuned by variation of the ion energy, dot diameters as small as 20 nm can be expected [29]. With respect to large area templates it has to be noted that ion bombarded nanostructured silicon surfaces [30] offer the possibility of template fabrication on commercially available 12 inch Si wafers. With metal seeding, Si dot sizes of about 20 nm are achievable [31, 32]. With resulting nanomagnet sizes below 20 nm more sophisticated strategies may have to be applied to overcome the superparamagnetic limit [33].

Finally it should be noted that the proposed fabrication of nanomagnet arrays on ion bombarded semiconductor templates not only has potential applications in data storage but in particular also for the emerging field of spintronics [34] and even for combining biomolecules with nanoelectronics [35]. Furthermore, the deposition method is completely general and non-material specific, so that it can also be used to obtain arrays of non-magnetic particles with applications in, for instance, catalysis or plasmonics.

## Acknowledgments

We wish to thank C Hofer and Z Seyidov for MFM measurements as well as M Á Niño, E Jiménez and J Camarero for magnetic deposition and MOKE measurements. Further, we are thankful to D Arvanitis and R Miranda for valuable discussions. This work has been supported by the European Community through the 'NAMASOS' project, no. NMP2-CT-2003-505854 and by bm:bwk Austria. Work by the Spanish group has also been partially supported by projects FIS2007-61114, MAT2004-0071-E, and CONSOLIDER-Ingenio en Nanociencia Molecular, Ref. CSD2007-00010. Support for researcher exchange from the Austria–Spain 'Acciones Integradas' programme through grant no. HU2003-0011 is acknowledged.

## References

[1] Martín J I, Nogués J, Liu K, Vicent J L and Schuller I K 2003 Ordered magnetic nanostructures: fabrication and properties *J. Magn. Magn. Mater.* **256** 449
[2] Teichert C 2002 Self-organization of nanostructures in semiconductor heteroepitaxy *Phys. Rep.* **365** 335
[3] Facsko S, Dekorsy T, Koerdt C, Trappe C, Kurz H, Vogt A and Hartnagel H L 1999 Formation of ordered nanoscale semiconductor dots by ion sputtering *Science* **285** 1661
[4] Teichert C 2003 Self-organized semiconductor surfaces as templates for nanostructured magnetic thin films *Appl. Phys.* A **76** 653
[5] Teichert C and Lagally M G 2007 Routes towards lateral self-organization of quantum dots: the model system SiGe on Si(001) *Lateral Alignment of Epitaxial Quantum Dots* ed O G Schmidt (Berlin: Springer) p 49
[6] Teichert C, Barthel J, Oepen H P and Kirschner J 1999 Fabrication of nanomagnet arrays by shadow deposition on self-organized semiconductor substrates *Appl. Phys. Lett.* **74** 588
[7] Mulders A M, Fraile Rodríguez A, Arvanitis A, Hofer C, Teichert C, Niño M Á, Camarero J, de Miguel J J, Miranda R, Lyutovich K, Kasper E, Heun S and Locatelli A 2005 Imaging of magnetic nano-dots on self-organized semiconductor substrates *Phys. Rev.* B **71** 214422
[8] Gridneva L, Persson A, Niño M Á, Camarero J, de Miguel J J, Miranda R, Hofer C, Teichert C, Bobek T, Locatelli A, Heun S, Carlsson S and Arvanitis D 2008 Experimental investigation on the spin reorientation of Co/Au based magnetic nano-dot arrays *Phys. Rev.* B **77** 104425
[9] Sekiba D, Moroni R, Gonella G, de Mongeot F B, Boragno C, Mattera L and Valbusa U 2004 Uniaxial magnetic anisotropy tuned by nanoscale ripple formation: ion-sculpting of Co/Cu(001) thin films *Appl. Phys. Lett.* **84** 762
[10] Bobek T, Mikuszeit N, Camarero J, Kyrsta S, Yang L, Niño M Á, Hofer C, Gridneva L, Arvanitis D, Miranda R, de Miguel J J, Teichert C and Kurz H 2007 Self-organized hexagonal patterns of independent magnetic nanodots *Adv. Mater.* **19** 4375
[11] Bradley R M and Harper J M E 1988 Theory of ripple topography induced by ion bombardment *J. Vac. Sci. Technol.* A **6** 2390
[12] Lauritsen K B, Cuerno R and Makse H A 1996 Noisy Kuramoto–Sivashinsky equation for an erosion model *Phys. Rev.* E **54** 3577
[13] Bobek T, Facsko S, Kurz H, Dekorsy T, Xu M and Teichert C 2003 Temporal evolution of dot patterns during ion sputtering *Phys. Rev.* B **68** 085324
[14] Facsko S, Bobek T, Stahl A, Kurz H and Dekorsy T 2004 Dissipative continuum model for self-organized pattern formation during ion-beam erosion *Phys. Rev.* B **69** 153412
[15] Xu M and Teichert C 2005 Size distribution and dot shape of self-assembled quantum dots induced by ion sputtering *Physica* E **25** 425
[16] Facsko S, Bobek T, Kurz H, Dekorsy T, Kyrsta S and Kremer R 2002 Ion-induced formation of regular nanostructures on amorphous GaSb surfaces *Appl. Phys. Lett.* **80** 130

[17] de Miguel J J, Cebollada A, Gallego J M, Ferrer S, Miranda R, Schneider C M, Bressler P, Garbe J, Bethke K and Kirschner J 1989 Characterization of the growth processes and magnetic properties of thin ferromagnetic cobalt films on Cu(100) *Surf. Sci.* **211/212** 732

[18] Meyer E, Hug H and Bennewitz R 2003 *Scanning Probe Microscopy. The Lab on a Tip* (Berlin: Springer)

[19] Cowburn R P, Adeyeye A O and Welland M E 1999 Controlling magnetic ordering in coupled nanomagnet arrays *New J. Phys.* **1** 16

[20] Mikuszeit N, de Miguel J J and Miranda R 2008 Anisotropy in two-dimensional arrays of collinear in-plane rotated identical particles with arbitrary charge or polarization distribution *Phys. Rev.* B **78** 054448

[21] Li Z G, Garcia P F and Cheng Y 1993 Co thickness dependence of the microstructure of Pt/Co multilayers *J. Appl. Phys.* **73** 2433

[22] Allenspach R, Stampanoni M and Bischof A 1990 Magnetic domains in thin epitaxial Co/Au(111) films *Phys. Rev. Lett.* **65** 3344

[23] Zhao Y, Wang G-C and Lu T-M 2001 *Characterization of Amorphous and Crystalline Rough Surface: Principles and Applications* (San Diego, CA: Academic)

[24] Albrecht M, Hu G, Guhr I L, Ulbrich T C, Boneberg J, Leiderer P and Schatz G 2005 Magnetic multilayers on nanospheres *Nat. Mater.* **4** 203

[25] Nakajima N, Koide T, Shidara T, Miyauchi H, Fukutani H, Fujimori A, Iio K, Katayama T, Nyvlt M and Suzuki Y 1998 Perpendicular magnetic anisotropy caused by interfacial hybridization via enhanced orbital moment in Co/Pt multilayers: magnetic circular x-ray dichroism study *Phys. Rev. Lett.* **81** 5229

[26] Chen Y J, Wang J P, Soo E W, Wu L and Chong T C 2002 Periodic magnetic nanostructures on self-assembled surfaces by ion beam bombardment *J. Appl. Phys.* **91** 7323

[27] Choi J, Wehrspohn R B and Gösele U 2005 Mechanism of guided self-organization producing quasi-monodomain porous alumina *Electrochim. Acta* **50** 2591

[28] Cheng J Y, Ross C A, Chan V Z-H, Thomas E L, Lammertink R G H and Vancso G J 2001 Formation of a cobalt magnetic dot array via block copolymer lithography *Adv. Mater.* **13** 1174

[29] Facsko S, Kurz H and Dekorsy T 2001 Energy dependence of quantum dot formation by ion sputtering *Phys. Rev.* **B 63** 165329

[30] Gago R, Vázquez L, Cuerno R, Varela M, Ballesteros C and Albella J M 2001 Production of ordered silicon nanocrystals by low-energy ion sputtering *Appl. Phys. Lett.* **78** 3316

[31] Ozaydin G, Özcan A S, Wang Y, Ludwig K F, Zhou H, Headrick R L and Siddons D P 2005 Real-time x-ray studies of Mo-seeded Si nanodot formation during ion bombardment *Appl. Phys. Lett.* **87** 163104

[32] Teichert C, Hofer C and Hlawacek G 2006 Self-organization of inorganic and organic semiconductor nanostructures *Adv. Eng. Mater.* **8** 1057

[33] Skumryev V, Stoyanov S, Zhang Y, Hadjipanayis G, Givord D and Nogués J 2003 Beating the superparamagnetic limit with exchange bias *Nature* **423** 850

[34] Prinz G A 1998 Device physics—magnetoelectronics *Science* **282** 1660

[35] Chang C-C, Sun K W, Lee S-F and Kann L-S 2007 Self-assembled molecular magnets on patterned silicon substrates: bridging bio-molecules with nanoelectronics *Biomaterials* **28** 1941